Research Square

Preprints are preliminary reports that have not undergone peer review.
They should not be considered conclusive, used to inform clinical practice,
or referenced by the media as validated information.

Flow-induced Folding in Multi-scaled Bulk Forming of Flanged Parts and its Prediction and Avoidance

Jun-Yuan Zheng
The Hong Kong Polytechnic University https://orcid.org/0000-0001-7711-5285
Jie Yi Chen Fang
The Hong Kong Polytechnic University
Ming Wang Fu (mmmwfu@polyu.edu.hk)
The Hong Kong Polytechnic University https://orcid.org/0000-0002-0409-9701

Research Article

Keywords: Flow-induced defect; geometrical size effect; finite element simulation; defect prediction and avoidance; multi-scaled forming

Posted Date: September 16th, 2021

DOI: https://doi.org/10.21203/rs.3.rs-879830/v1

License: This work is licensed under a Creative Commons Attribution 4.0 International License.
Read Full License

Flow-induced Folding in Multi-scaled Bulk Forming of Flanged Parts and its Prediction and Avoidance

Jun-Yuan Zheng, Jie Yi Chen Fang, Ming Wang Fu *

Department of Mechanical Engineering, The Hong Kong Polytechnic University, Hung Hom, Kowloon, Hong Kong SAR of China

* mmmwfu@polyu.edu.hk

Abstract

The quality of manufactured parts and the efficiency of forming processes are crucial in deformation-based manufacturing. In product miniaturization and micro-manufacturing, size effect induces many unknowns. Flow-induced folding related to size effect is one of them and has not yet been fully studied. In this research, the formation mechanism of folding defects in axisymmetric bulk forming was investigated, and a design-based method was employed to evaluate different tooling and process route designs for making a case-study multi-flanged part with three features and to explore the design-based avoidance of folding defects. In addition, a design evaluating framework of folding-free bulk forming was proposed, implemented and validated. Via analysis of the material flow, energy consumption, folding formation, and product precision of the four proposed forming processes for the case-study part, an upsetting-extrusion forming method via using a nested punch was found to be the most desirable. It was then implemented in the physical forming with three size scales. The results revealed that the flow-induced folding in the macropart was severe and regularly circuitous, but it is slight and irregular in meso and microscale. These findings are useful in the defect-free forming of multi-flanged structures and multi-scaled axisymmetric parts.

Keywords: Flow-induced defect; geometrical size effect; finite element simulation; defect prediction and avoidance; multi-scaled forming

1. Introduction

Ductile-metal forming is widely used to produce net-shape or near-net-shape parts and components via plastic deformation of materials since it has many advantages such as efficient productivity, high material utilization, excellent mechanical properties, the good manufacturability of forming complex shapes, and low cost of mass production [1, 2]. Metal-formed parts generally require high properties and defect-free quality to have a good service performance. However, due to imperfect tooling, severe plastic deformation, overlarge stress, and complex material flow, forming defects are common in metal-formed parts. Defects in metal forming can be classified according to the original forming modes into two groups, viz., sheet-forming defects and bulk-forming defects. In sheet metal forming, materials mainly deform under tensile and shear stresses, thus stress-induced cracks are the major defect type, such as cracks on the corner in the incremental-formed parts [3-5] and cracks on the upper edge [6, 7] and bottom [8, 9] of the deep-drawn cups. Moreover, wrinkling occurs in complex-shaped sheet metal forming due to the unstable and unreasonable blank holding force and the uneven stress [10]. By contrast, compressive deformation is a major deformation mode in bulk metal forming, and the defects are mainly induced by undesirable material flow. Prior researches were more focused on the defects in forging process. Arentoft and Wanheim [11] identified the defects in forging and classified them into several groups, including crack, surface defect, form defect, shear defect, structural defect, and folding. Balenda and Qin [12] classified the flow-induced defects in injection forging into fracture, buckling, folding, underfilling/notch, and thinning/unevenness. However, the flow-induced defect is a primary defect type since ductile fracture barely happens at the negative stress triaxiality [13]. The sub-classification of flow-induced defects can be summarized by buckling, folding, underfilling, and unevenness. Some examples of flow-induced defects are illustrated in **Fig. 1**. In **Fig. 1** (a), buckling occurs when a thin-walled ring is upset to be thicker in the die cavity without lateral constraint [14]. In **Fig.**

1 (b), the folding happens when the punch shoulder compresses the back-extruded material [15]. Moreover, **Fig. 1** (c) shows a tooth underfilling in the first tooth indentation, which is induced by a large amount of localized plastic deformation [16]. **Fig. 1** (d) illustrates a geometrical unevenness in cold pin-head embossing when the distance between the punching position to the edge is too small [17].

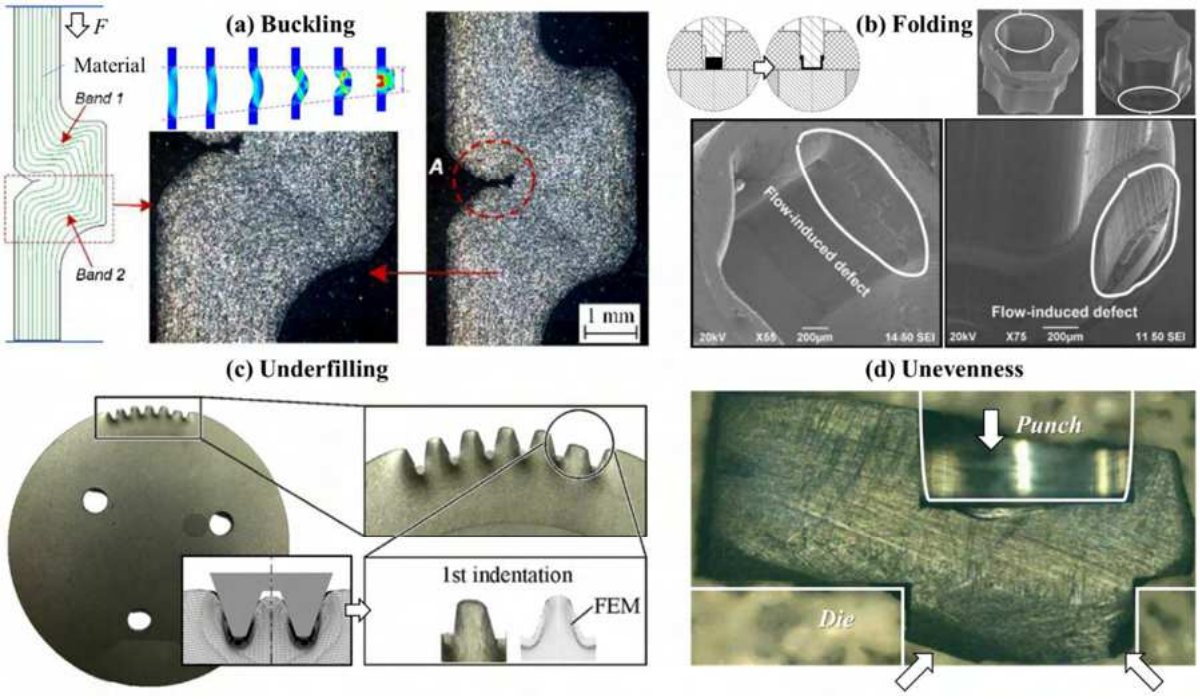

Fig. 1 Flow-induced defects in different bulk metal forming processes. (a) Buckling in the ring upsetting [14]. (b) Folding in the flange extrusion [15]. (c) Underfilling in the incremental gear forming [16]. (d) Unevenness in the pin-head embossing [17].

Among the flow-induced forming defects, buckling and folding have a similar formation mechanism. When there are material flows from two or more directions under compressive stress, the localized material streams in merging joint tend to flow in different directions, where the material buckling happens. With buckling development, however, the material surface self-contact emerges, and the original external material surface becomes the internal contacted surface inside the deforming workpiece without bonding, where the folding happens. For an axisymmetric part, a “V” shaped profile or a sideways deflection is generated and closed at this

merging region, and folding happens at the self-contact region. Therefore, the direct solution for folding is to constraint and control the flow merging when the workpiece is bulging, forging, upsetting, or to avoid these forming operations by improving tooling design [18, 19] and optimal design of process route [20, 21]. Folding is one of the most important flow-induced defects that can always cause stress concentration in product service and greatly influences the quality and service performance of the deformed parts. Deep folding can be hardly eliminated or avoided in the subsequent processes. The mechanism and avoidance of folding defects were studied by many researchers. Chan et al. [21] analyzed the mechanism of folding and developed a die structure with a spring-assisted insert to avoid the formation of folding. Chan et al. [20] further investigated the relative geometrical parameters and their sensitivities to folding defects in axisymmetric flanged components. Sun et al. [22] investigated the relationship of folding defect and loading path in forming of complex structures by numerical and physical simulations. Gao et al. [23] developed a quick prediction model to evaluate the possibility and severity of folding defects in rib-web forming by using an adaptive folding index. Gao et al. [24, 25] further divided the folding defects into three types, viz., confluence-type, bending-type, and local-loading-type according to material flow characteristics and analyzed their formation mechanism and sensitivity. A prediction approach was then proposed based on folding indexes, criteria, and models. Hsu et al. [26] developed a multi-stage warm forging process and found the formation of folding in a deep groove ball bearing. Wang et al. [27] investigated the folding defect in meso-forming processes and developed a folding-free approach by changing the forming sequence of part features. Wang et al. [28, 29] investigated geometrical and grain size effects on the formation of flow-induced defects in multi-scaled flanged parts and found that the decrease of geometry size can significantly reduce the folding defects. Liu et al. [30] developed a simulation-based method to determine the thickness and location of folding in a hot-forged automotive shaft and avoided its formation by optimized tooling design.

From the above literature review, it is known that folding defects can be adequately avoided by controlling material flow and optimizing the design of tooling and process. Investigating the formation and mechanism of folding is critical for predicting and avoiding it in bulk metal forming. With product miniaturization, micro-scaled metal forming technologies have become popular and are widely used in industries. However, the knowledge and experience about the avoidance of folding defects in macro-scaled forming are not in-depth or sufficient enough. Research on the mechanisms of flow-induced defects in meso/microforming is also limited. This study thus focuses on the mechanism of folding defects related to the material flow affected by size effect in axisymmetric bulk forming. Four improved scenarios for tooling design and process route design were proposed to avoid the formation of folding defects in an axisymmetric multi-flanged part, and a general design analysis framework for evaluating the designed part, tooling, and process route was developed for folding-free bulk metal forming. Through analysis of material flow, strain distribution, and comparison of the load-stroke curves of the proposed cases, the best design was identified.

2. Folding defects in axisymmetric bulk-formed parts

2.1 Classification and formation mechanism of folding defects

Common axisymmetric bulk parts can be classified into hollow and solid types according to whether they have a central hole or not. **Fig. 2** illustrates the formation of two types of folding in hollow and solid parts. Folding is a typical defect in compressive deformation in forming of axisymmetric hollow bulk parts, as shown in **Fig. 2** (a). During ring compression, material generally flows in multi-directions and outward against the central axis. But due to the constraints, viz., friction and die cavity, the material flow near the contact surface with punch is usually hysteretic. There are thus uneven material flows that easily induce the flow turbulence

and undesirable flow merging to form the folding on the inner surface. This type of folding is named as flow-induced folding. To avoid this folding in hollow parts, the laterally constrained material flow is needed. However, a diameter-flexible constraint on the lateral surface of axisymmetric parts is impossible. Zhu et al. [14, 31] proposed a novel method to transfer this constraint to an axial constraint by pushing the material from a holding cavity to a forming cavity with a movable counter punch, which can efficiently avoid the folding in upsetting of hollow part. By contrast, for forming of solid parts, flow-induced folding is uncommon, but another folding type still remains, which is named as structure-induced folding, as shown in **Fig. 2** (b). If a bulk part has a concave lateral profile, such as conner, groove, and stepped feature on the material cylindrical surface, the concave feature will have a chance to be closed via the merging of material flows from top down and bottom up in upsetting process. By analyzing the forming mechanisms of folding, an efficient and economic way for folding avoidance is to improve the tooling and process design to tailor and control the material flows in deformation process.

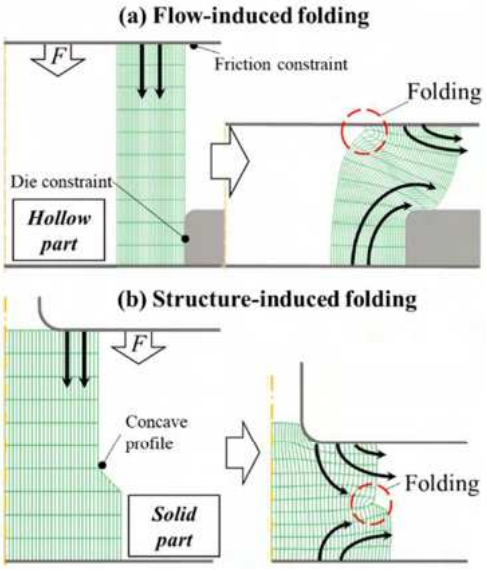

Fig. 2 Folding defects in axisymmetric metal forming: (a) Flow-induced folding caused by the uneven lateral material flows; (b) Structure-induced folding induced by the concave profile on the preform.

The incoordinate lateral material flow during upsetting is the major cause of the localized material flows in hollow axisymmetric parts. To investigate this effect, ring upsetting simulations with different interfacial friction were established, as shown in **Fig. 3**. When the interfaces are both frictionless, as shown in **Fig. 3** (a), the billet deforms evenly and no folding or curved surface occurs. When the friction factor is 0.1 as a good lubricated condition, as shown in **Fig. 3** (b), the inner surface is slightly curved but no folding occurs. However, in dry conditions with a friction factor of 0.7, as shown in **Fig. 3** (c), the inner surface is fluctuant and the middle area is thus potential to be folded. Moreover, when the lubrication on the two interfaces is different, as shown in **Fig. 3** (d), folding more easily occurs near the lubricated die. Therefore, in hollow part upsetting process, poor and different interfacial lubrication of top and bottom dies should be avoided.

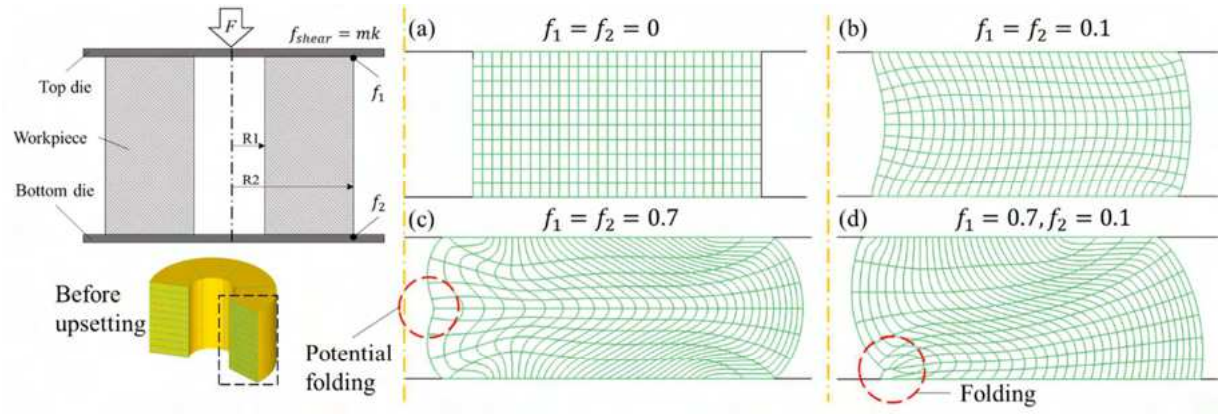

Fig. 3 The influence of friction on folding defects of ring upsetting with different friction factors on the interface of top die and bottom die.

2.2 Folding formation in axisymmetric flanged forming

The conventional forming of an axisymmetric flanged part with a central hole has a high risk of folding, where the billet is compressed to form the designed shape in one stroke by punch and die with the designed multi-stepped profiles. In forming of hollow parts, however, a stepped punch is usually used in one-stroke forming, and folding is usually related to the multi-extrusion of the hollow feature. **Fig. 4** presents a conventional forming process for axisymmetric multi-

flanged parts. Generally, to form the part in one stroke, the punch and die used in this process are designed directly based on the shape of the part's inner and outer geometries. The one-stroke forming is divided into backward-extrusion and upsetting stages, and the folding appears at the upsetting stage, as shown in **Fig. 4** (a). **Fig. 4** (b) presents the material flow pattern at the upsetting stage. At this stage, the head and shoulder of the moving punch are two portions pushing the material to flow. The first contact is the place where the punch head pushes the material to flow backward along the die surface. The flow streams are separated into two directions near the die edge. The major flow direction is still backward, and the minor flow direction is lateral. By contrast, the second contact is located at the place where the punch shoulder pushes the backward-flowing material into two flow directions as it is sufficiently extruded. The two nearly opposite inward flows merge and form a serious folding defect. The two outward flows fill up the space of die cavity and no folding defect is formed.

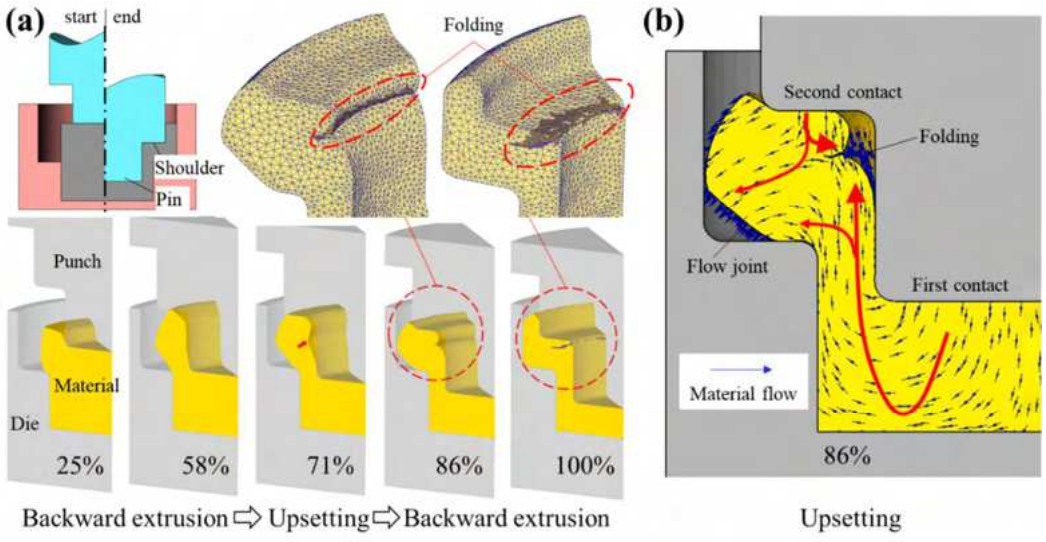

Fig. 4 (a) Folding formation process in one-stroke flanged forming. (b) The material flow pattern at the 80% stroke.

3. Simulation-enabled tooling and process route designs: a case study

3.1 Folding defect in multi-flanged parts

Multi-flanged parts with three size scales were studied using cold metal-forming processes to investigate the formation of folding defects and how to avoid them. The formed parts are shown in **Fig. 5** (a). The part design is illustrated in **Fig. 5** (b), and it is identified by three features based on its geometrical shape, where Feature A is the peak outer ring formed by backward extrusion, Feature B is the flat shoulder forged and extruded from cylindrical billets, and Feature C is the central hole formed by punch extrusion. The detailed dimensions of the flanged part at the three scales are shown in **Table 1**. The three scales are identified by the "scale factor" to show their multiplied relationship. According to their dimensional ranges, "1" represents the microscale, "2" represents the mesoscale, and "4" represents the macroscale.

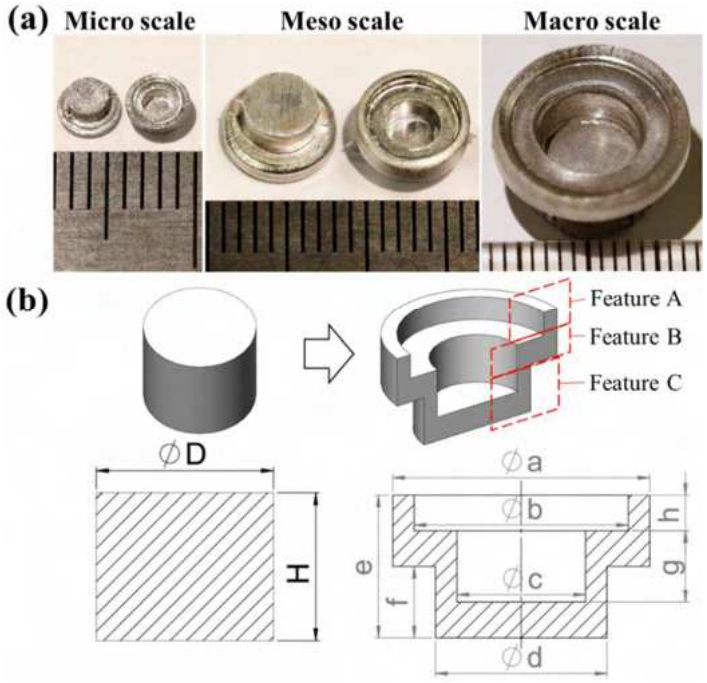

Fig. 5 (a) The multi-flanged parts with three size scales and (b) the design of billets and parts with three features.

Table 1 Dimensions of parts with three size scales.

	Dimensions (mm)									
Scale factor	D	H	a	b	c	d	e	f	g	h
1 (Micro)	2.4	1.8	3.6	3	1.8	2.4	2	1	1	0.35
2 (Meso)	4.8	3.6	7.2	6	3.6	4.8	4	2	2	0.7
4 (Macro)	9.6	7.2	14.4	12	7.2	9.6	8	4	4	1.4

The flow-induced folding defects are easily observed in the one-stroke formed parts at all three scales, as shown in **Fig. 6**. The figure shows that the location of the folding defect is near the edge of the inner surface of Feature B in experiments, which is consistent with the simulation results shown in **Fig. 4**.

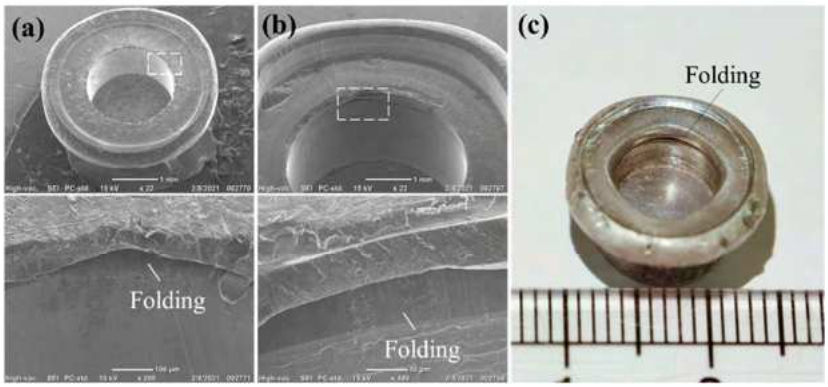

Fig. 6 Folding defects in the flanged (a) micro-, (b) meso- and (c) macro-scaled parts caused by the one-stroke forming process.

3.2 The optimized method to folding avoidance

A framework for folding-free forming process design and folding defect analysis, prediction, and avoidance was proposed, and is illustrated in **Fig. 7**. The beginning of the framework is conceptualization with the input of voice of customers, which defines the design specifications and functional requirements of the part to be fabricated. The conceptualization is then detailed with the specific part design, including part dimensions, geometry features, relative tooling

shapes, and a processing route. Once a design is proposed, its formability analysis is conducted through FE simulation. If the design is defective, folding avoidance methods for design improvement should be considered. The framework provides process control and design-based methods, as shown in **Fig. 7**.

(1) For the process control method, the specific folding location of the critical feature and its occurring step should be determined first. This method requires strict tooling constraints to control material flows without flow merging during the critical feature forming. Based on these additional requirements, forming tooling is redesigned.

(2) For the design-based method, when and where the folding initiates need to be figured out first, and the folding type is determined. If the folding is structure-based, the forming route should be revised to avoid the compressive deformation of the critical feature, such as concave structures. On the other hand, if the folding is flow-induced, the forming process should be optimized to avoid direct upsetting of thin-wall or slender material. Based on the improved forming route and process sequence, the forming tooling is redesigned.

The folding analysis, prediction, and avoidance methods result in the redesign of tooling, and the formability analysis of the new design should be conducted once again. If the new design is defect-free, the project can be implemented.

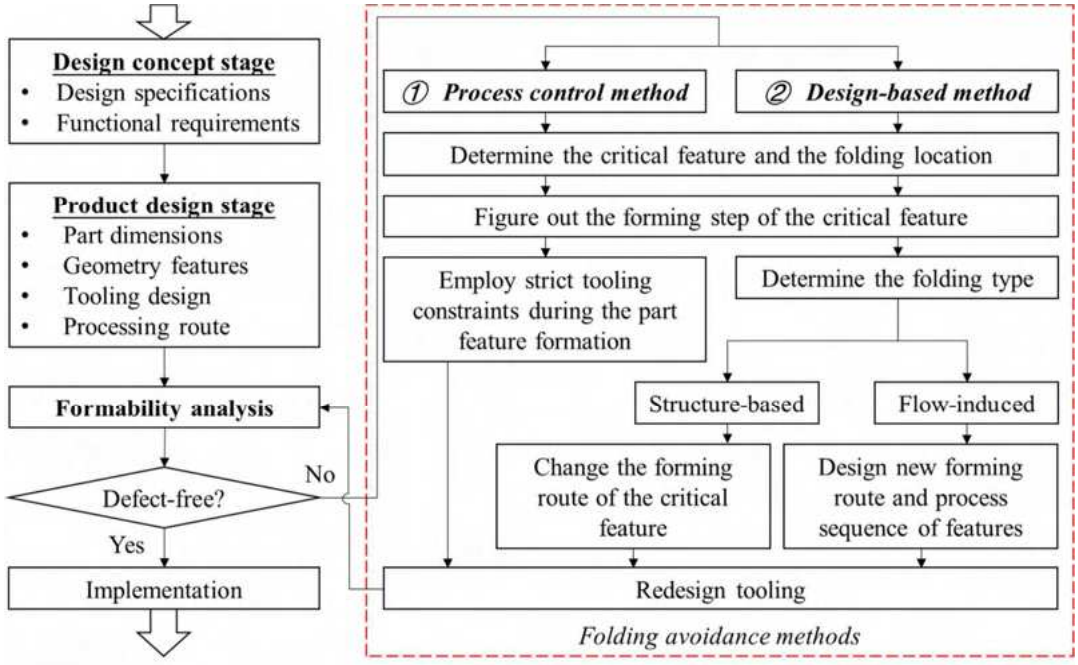

Fig. 7 Framework of folding defect analysis, prediction, and avoidance in forming processes.

3.3 Improved designs of the multi-flanged part for folding avoidance

The studies on the one-stroke multi-flanged forming reveal that the folding defects are primarily caused by the merging of material flows from multi-directions during the forming process. Thus, the design-based approach for avoiding folding is to eliminate the merging of material flows. This section discusses tooling and process route designs for improving the material flow during the multi-flanged forming, as shown in **Fig. 8**.

3.3.1 Case 1

This case uses a stepped punch with a shortened punch head. With the punch stroking, a part of Feature C and the whole of Feature B are formed. After this forming, the punch is replaced by a hollow holder with a movable insert. By moving the insert, Feature A and the left of Feature C are formed.

3.3.2 Case 2

This case first uses a flat punch to forge a cylindrical billet into a plug shape. Feature B is partially formed. The flat punch is then replaced by a fixed holder with a movable insert, and

the insert moves downward for extrusion. Features A and C are formed simultaneously.

3.3.3 Case 3

This case employs a flat punch and a flat movable die inserted in a hollow die. First, the movable die is fixed, and the flat punch compresses the cylindrical billet. Features A and B are formed after upsetting and backward extrusion. Thereafter, the flat punch is replaced by a hollow holder with a movable insert. The movable insert punches downward and the flat movable die moves down at a relative speed of the insert. Feature C is formed after the metal drawing deformation.

3.3.4 Case 4

This case applies a die with a spring-supported sliding insert [21]. The sliding insert raises the separating position of material flow in backward extrusion. When the punch shoulder contacts the material, the sliding insert is pushed down by the material to the designated strokes. Feature C is formed. Thereafter that, the punch is replaced by a punch with a thinner shoulder. With the punch moving, Features A and B are formed from billet.

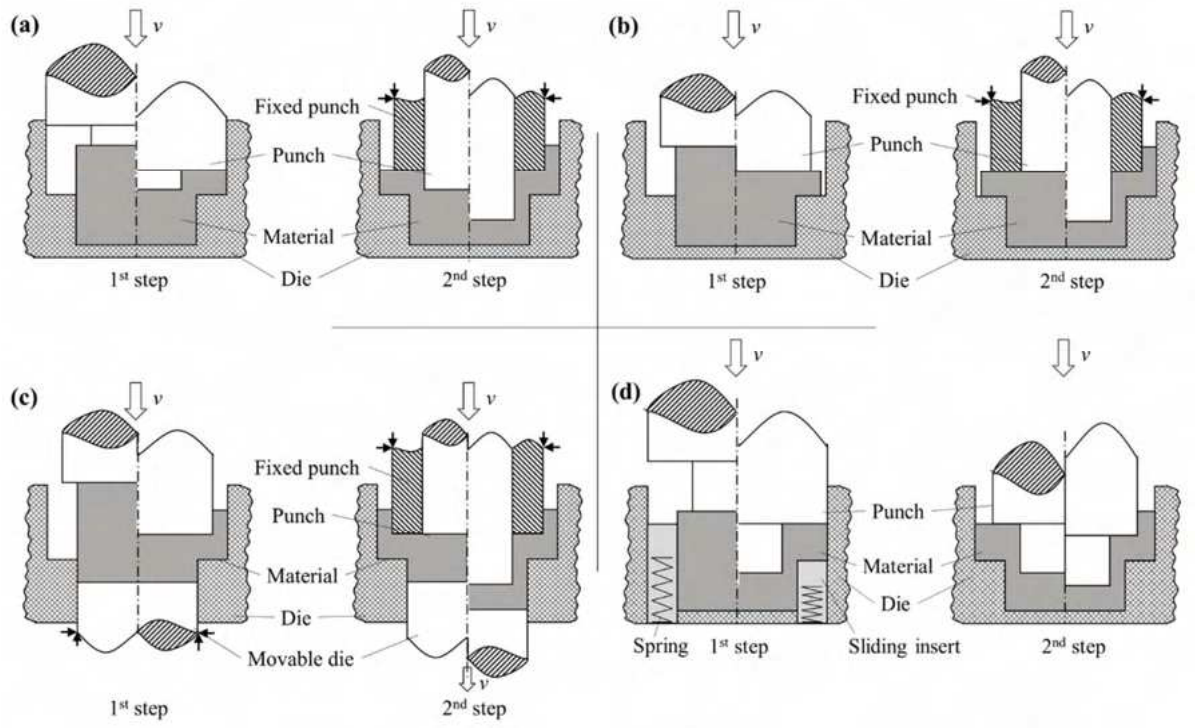

Fig. 8 Improved two-step multi-flanged forming processes. (a) Case 1: shortened-head design; (b) Case 2: flat-punch design; (c) Case 3: movable-die design; (d) Case 4: slidng-insert design.

3.4 Experimental material and its properties

Aluminum alloy AL1060 (Al ≥ 99.60%) was used as the experimental material in this study due to its excellent ductility and homogeneous textures. The material was annealed at 400 °C for 1 hour under an argon-filled furnace to release the work hardening and then gradually cooled down to room temperature. To obtain the mechanical properties of AL1060, uniaxial tensile tests were conducted at room temperature using an MTS testing machine with a 10-kN-capacity load cell. Dog-bone-shaped tensile specimens were used and repeated four times. The strain rate was 0.01 s^{-1}. Thus, the rate effect could be ignored. The dimensions of specimens and the flow stress curves are shown in **Fig. 9**.

The Swift model [32] is a well-known empirical model used to describe the flow stress of materials and is designated as a power law as follows:

$$\sigma = C(m + \varepsilon)^n \tag{1}$$

where σ is flow stress, ε is plastic strain, and C, m, and n are the empirical constants fitted from experimental data. The parameters and mechanical properties are summarized in **Table 2**. The model was employed in simulation to describe the mechanical responses of the material.

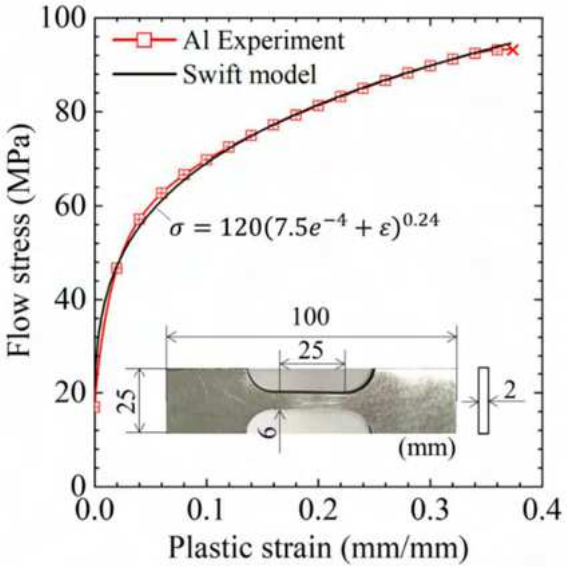

Fig. 9 Flow stress of the testing aluminum alloy.

Table 2 Mechanical properties of the annealed aluminum alloy AL1060.

AL1060 properties			Swift model		
Young's modulus	Poisson's ratio	Yield stress	C	m	n
69 GPa	0.33	17 MPa	120 MPa	7.5×10^{-4}	0.24

3.5 Development of multi-scaled forming systems

To comprehensively evaluate the feasibility of the four proposed designs in Section 3.2, simulation-based studies of the four forming processes were conducted using a FEM simulation system. The tooling sets were used in both the conventional one-stroke forming and the two-step forming in Case 2, as shown in **Fig. 10** (a). The punch contains a sleeve and a pin, and a gasket is used to shift their relative position to realize the required operation. Regarding the one-stroke forming, the punch pin is pressed down of the punch sleeve to create a stepped punch, as shown in **Fig. 10** (b). In the first step of the two-step forming, the punch pin and the punch sleeve are assembled to a flat punch by using the gasket. Then the gasket is taken out, the sleeve is fixed, and the pin punches in the second step, as shown in **Fig. 10** (c). Regarding the simulation, the one-eighth billet with 40,000 tetra mesh was used with symmetrical boundary conditions. The shear friction model with a coefficient of 0.4 was applied to describe the interfacial friction between aluminum and steel tooling. For example, **Fig. 10** (d) presents the simulation setting of Case 2.

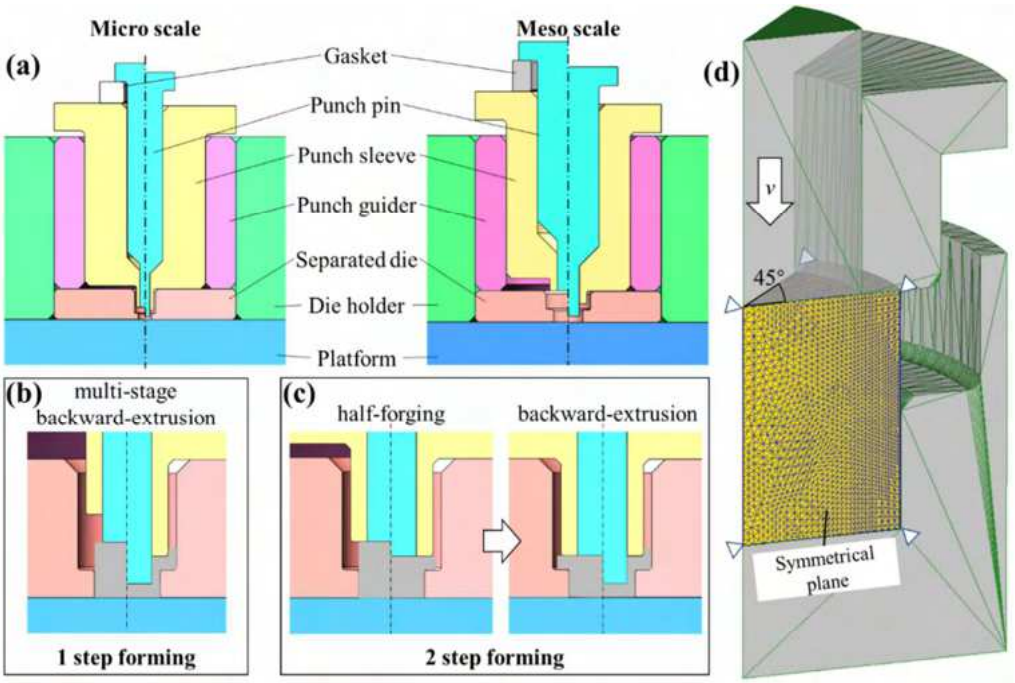

Fig. 10 (a) The tooling structures of the multi-scaled forming system. (b) The forming illustration of the original one-stroke process. (c) The forming illustration of the two-step process of Case 2. (d) The simulation setting of Case 2.

The multi-scaled forming experiments were conducted to investigate geometrical size effect on the formation and avoidance of folding defects. An MTS test machine with a load cell of 50 kN was used. The stroke velocity of the crosshead was 0.01 mm/s to avoid the influence of the strain rate. The interfaces of billet and tooling were lubricated using machine oil to reduce friction. The manufactured tooling sets are shown in **Fig. 11**. The separated dies and die holders are applied for easier ejection. The separated dies and punch guider are inserted in the die holder and fixed by the platform. Considering the gaps between the platform and the separated dies, the billets with slightly bigger dimensions of $\emptyset 2.4 \times 2$, $\emptyset 4.8 \times 4$, and $\emptyset 9.6 \times 8$ mm are prepared.

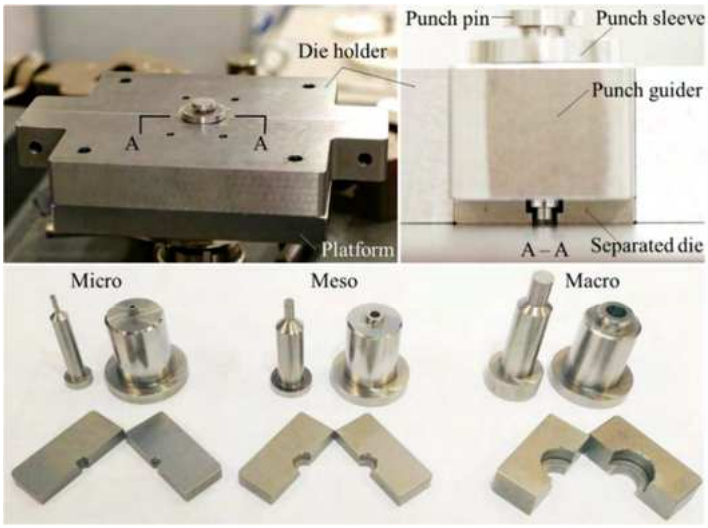

Fig. 11 The tooling sets of the multi-scaled forming system.

4. Results and discussion

4.1 Forming process analysis

The normalized load-stroke curves of the three size-scaled parts for the one-stroke multi-flanged forming are presented in **Fig. 12**. Among different size-scaled forming processes, the normalized load is defined as the current load divided by the square of their relative scale factor, and the normalized stroke is defined as the current stroke divided by their relative scale factor, as follows:

$$\begin{cases} Normalized\ load = \dfrac{Load}{Scale\ factor^2} \\ Normalized\ stroke = \dfrac{Stroke}{Scale\ factor} \end{cases} \tag{2}$$

From **Fig. 12**, it is found that the entire forming process can be divided into three stages. In the first stage, the punch head presses the upper surface of the billet, and the upper half of the billet begins to be extruded backward without any lateral constraint. When the extruded material contacts the punch shoulder, the second stage begins. The material is continuously extruded backward by the punch head and then upset laterally by the punch shoulder. The flow-induced folding is formed during this stage due to the bending of the extrudate. Since the contact area

between the punch and material increased, the normalized force rises rapidly. When the material reaches the inner cylindrical surface of the die, the third stage starts. The material is extruded by both the head and shoulder of punch and flows backward to form Feature A. The third stage ends when the punch reaching the designated stroke.

The normalized load-stroke curves show a similar trend for different size scales, but the meso-scaled curve gets the maximum normalized load. The curves for microscale and macroscale are close to that of the mesoscale in the first stage. According to surface grain theory [33], the grains located on the specimen surface show lower strength, so the flow stress of the specimen decreases with the specimen size. On the other hand, due to the effects of open and closed pockets on the lubricated interfaces [34], a larger surface area induces a better condition and further a lower forming load. Influenced by the above mechanisms, the maximum normalized load at the meso-scaled case is obtained.

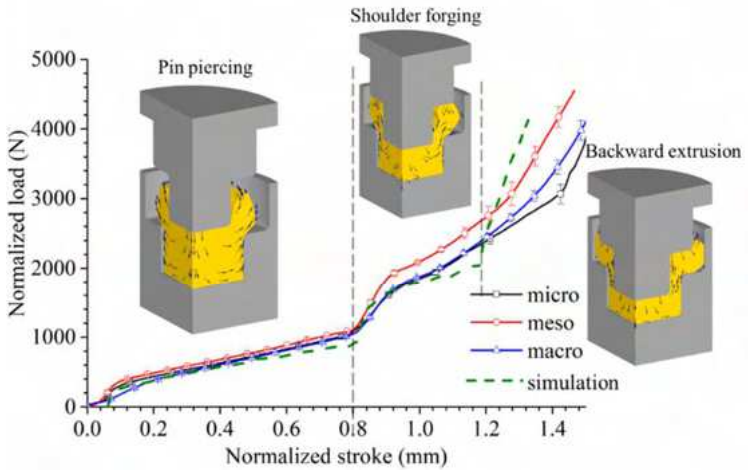

Fig. 12 Normalized load-stroke curves of the three size-scaled physical forming processes and the simulation.

The load-stroke relationship in the deformation process of Case 1 is shown in **Fig. 13**. The total stroke is 1.3 mm, where the sub-stroke is 0.87 mm for the first step and 0.43 mm for the second. For the first step, the punch head is shortened from 1 to 0.57 mm following the volume-constant

principle. The material is pushed to flow upward and then laterally once the material contacts the punch shoulder. Thus the forming load is suddenly increased at this time. When the material contacts the inner surface of the die, the material reflows to fill the unfilled space between punch and die, resulting in a sharply increased forming load. Thereafter, the second forming step begins. The punch is replaced by an insert punch and a fixed holder with a gap to the die surface. The insert punch pushes the material to flow backward to form Feature A until the punch reaches the designated position, and the maximum forming load of 4,430 N is obtained.

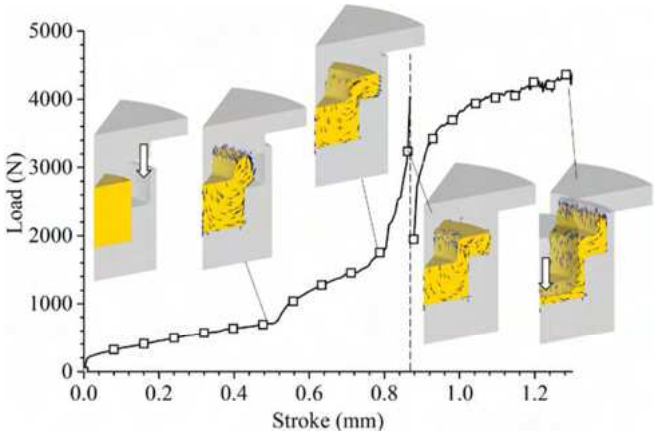

Fig. 13 Load-stroke curves of Case 1 determined by simulation.

The normalized load-stroke curves of the two-step deformation process of Case 2 with differently size-scaled experiments and simulations are presented in **Fig. 14**. The entire stroke is 1.3 mm, and 0.3 mm for upsetting and 1 mm for backward extrusion. The punch is comprised of a holder and an insert. For the first step, the holder and the insert move simultaneously to compress the upper half of billet. Once the first step is finished, the holder is fixed, and the insert continuously presses the material for extrusion. The material first flows laterally to fill the space of the die and then flows upward along the gap between the holder and die. At the stage of upward flow, the simulation result is clearly different from the experimental results.

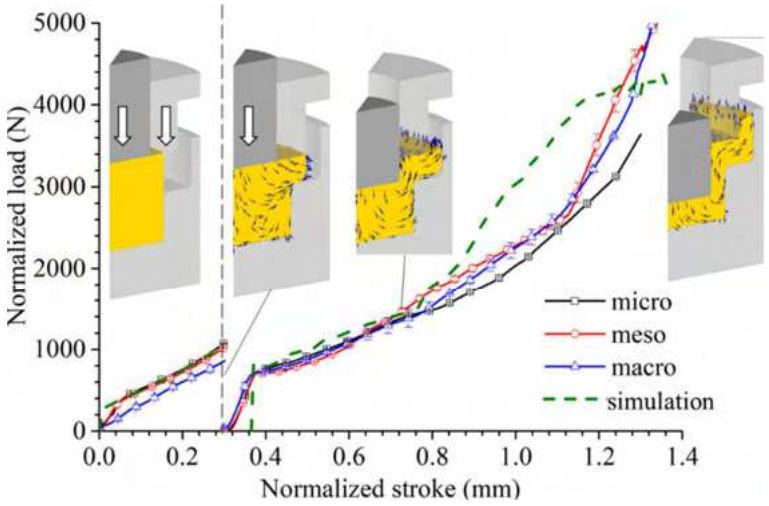

Fig. 14 Normalized load-stroke curves of Case 2 determined by experiment and simulation.

The load-stroke curve of Case 3 determined by simulation is illustrated in **Fig. 15**. The whole stroke is 1.8625 mm and is divided into two steps. The first step is an upsetting-backward extrusion step with a stroke of 0.8625 mm, while the second step is a drawing step with a stroke of 1 mm. In the first step, the load is first increased gradually with punch stroking. A small part of the billet is fixed using the hollow die, and the other part is forged and bulged by the flat punch. Once the material contacts the die surface, the material flows backward along the gap between the punch and die, resulting in a suddenly increasing load. When the punch reaches the designated position, the maximum load is obtained, which is 3,114 N. In the second step, the flat punch is replaced by a holder and a punch insert. The second step is a metal-drawing process, where the die insert is no longer fixed but moves relatively with the movement of the punch insert. The deformation load in this step is steady until the desired feature is formed.

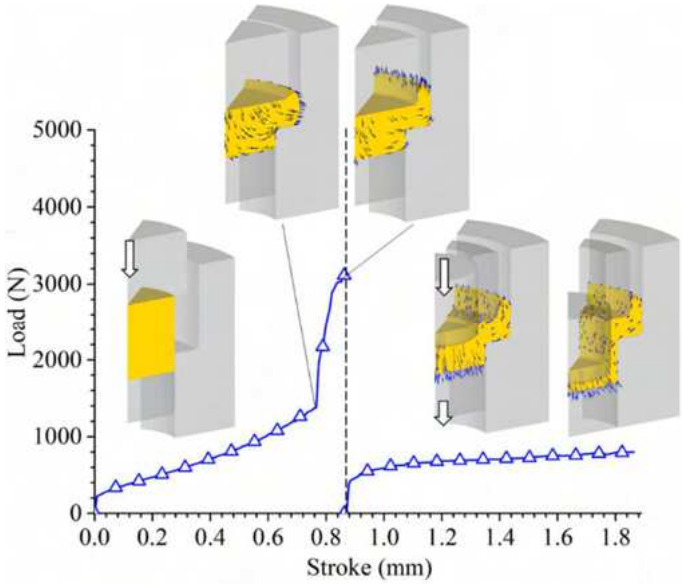

Fig. 15 Load-stroke curves of Case 3 determined by simulation.

The load-stroke and slider stroke curves of the slider during the forming process in the simulation of Case 4 are shown in **Fig. 16**. The stroke is 1.3 mm in total, with 1.16 mm for a slider-assisted extrusion and 0.14 mm for a backward extrusion. Initially, the billet is compressed by the punch head to flow upward. When the material contacts the shoulder of the punch, the vertical gap between the slider and the punch shoulder is approximately equal to or slightly smaller than the thickness of the extrudate to avoid the occurrence of folding defects. The extrudate is then extruded into the gap, and the load is rapidly increased due to the increased contact area. Meanwhile, the slider moves down gradually with the extrusion. The gap is filled by the material, and then the gap filler expands until its thickness reached the designated value. Thereafter, the punch is changed to a thinner stepped punch, which pushes the material to form Feature A and B until the slider reaches the maximum stroke. The maximum load is 4,940 N.

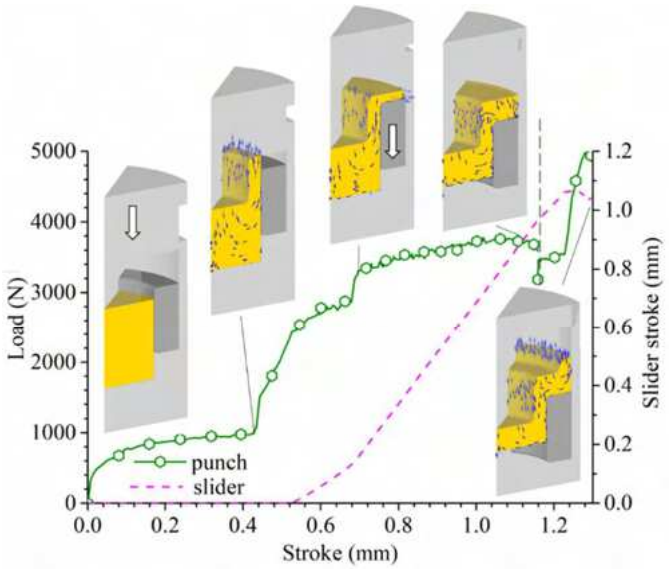

Fig. 16 Load-stroke curves and the slider stroke of Case 4 determined by simulation.

To quantitively evaluate the efficiency and resource consumption of the four cases, the comparison of the consumed energy, maximum load, and the total stroke during the forming processes are shown in **Fig. 17**. **Fig. 17** (a) reveals that Case 3 has the lowest consumed energy and the maximum load, which means it is the most economic and demands less for equipment. Meanwhile, Cases 1 and 2 have the similar values of the energy consumption and the maximum loads due to their similar deformation processes. Since the spring of slider stores elastic potential energy, Case 4 has the largest energy consumption and the maximum load. However, **Fig. 17** (b) shows that Case 3 has the longest total stroke, revealing that it requires more time to form a final part with the same forming rate.

In summary, both Cases 2 and 3 are desirable process for the two-step forming of a multi-flanged part. Concerning energy consumption and equipment requirement, Case 3 is more desirable; concerning production efficiency, Case 2 is more desirable.

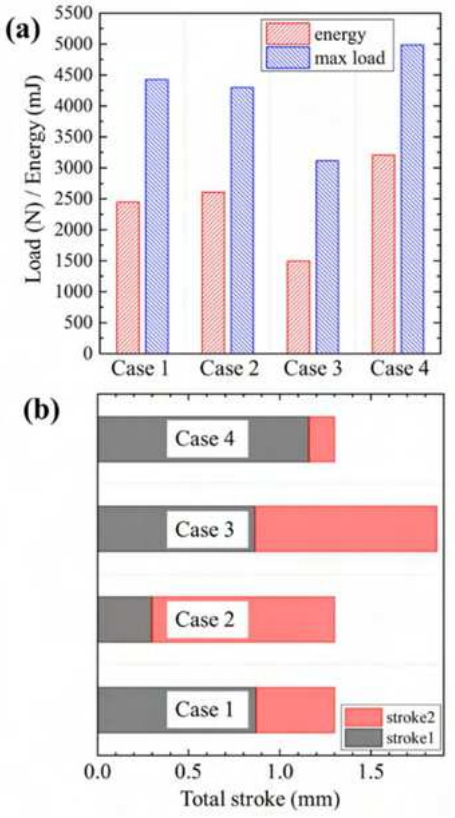

Fig. 17 (a) The consumed energy and maximum load of Cases 1 to 4. (b) The total and separated strokes of Cases 1 to 4.

4.2 Forming quality of final parts

The forming quality of different cases is evaluated according to the simulated stress and strain distributions and freeform dimensions. The effective strain distributions in the four formed parts are illustrated in **Fig. 18** (a–d). The figure shows that the strain is generally concentrated on the inner hole. In Case 1, however, a large strain band appears on the upper half of the inner hole. In Case 4, shear bands appear on the upper half of the inner hole and the inner surface of Feature A. High strain is generally induced by severe deformation, which increases the possibility of fracture. In addition, the folding defect in Case 1 cannot be fully avoided, as shown in **Fig. 18** (a). At the 65% stroke, the material is pushed to flow back, causing the merging of material flows, and then the folding defect is formed. On the other hand, the bottom edge of the parts in Case 3 shows a different geometry from that in other cases, as shown in **Fig. 18** (e). The curved

bottom edge of Case 3 is induced by the metal drawing process. In other cases, the billet is inserted and compressed at the die cavity to form a square edge with strain concentration.

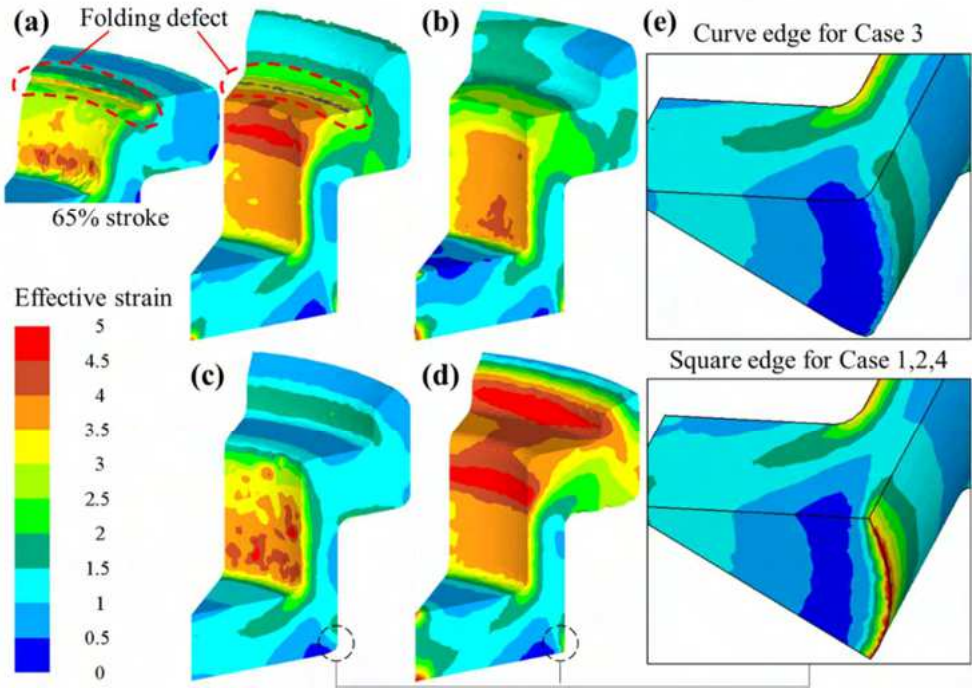

Fig. 18 Effective strain distribution of the simulation results of (a–d) Cases 1 to 4; (e) different shapes of the bottom edge

To investigate the formation of folding defects in Case 1, the punches with various head lengths were used to conduct simulations, and the results are shown in **Fig. 19**. The flow pattern illustrates the material flow behaviors when the first stroke is nearly finished. The figure shows the material is first pushed by the punch head to flow into lateral and upward directions to fill the cavities, and the material is then compressed by the punch shoulder to flow laterally. The corners of punch and die are the last to be filled. The folding defect occurs while the material filling the punch corner. By changing the head length, the profile shapes of the material during the punch corner filling are different. The cavity of the punch corner is in a right triangular shape, and the hypotenuse is generally curved. Due to the interfacial friction between the material and punch, the material at the punch shoulder deforms delayingly. However, the

material near the punch head tends to flow inward, while the material near the punch shoulder tends to flow outward. The dip angle θ, defined as the angle between material and punch head, as shown in **Fig. 19**, is decreased as the length of the punch head is increased. When θ is over a critical point, the likelihood of a folding defect occurring is increased. When *m/n*, which is defined as the ratio between the length of the shortened head to the original head, is larger than 55%, the folding defect occurs.

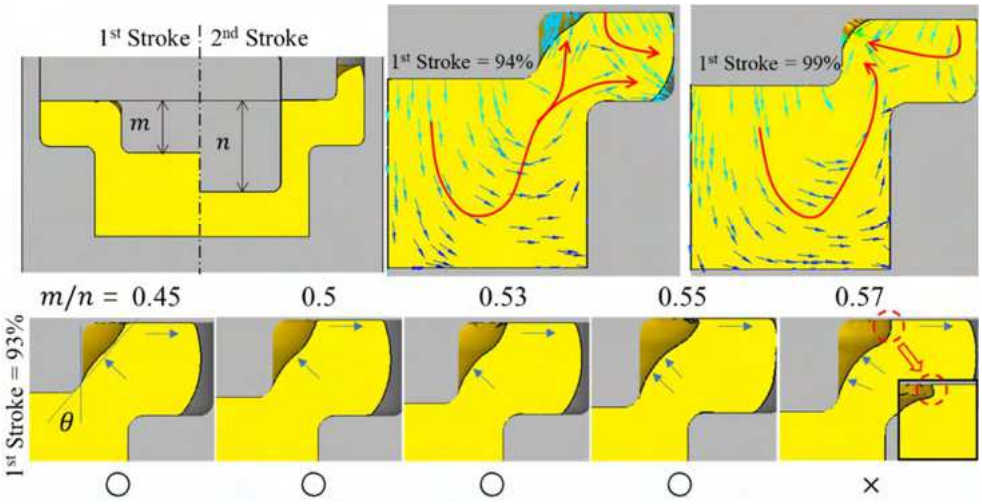

Fig. 19 The formation of a folding defect in Case 1.

The distributions of effective stress after the first and second strokes of different cases are shown in **Fig. 20**. It is shown that Case 4 has a large area of high stress due to the reactive force of the sliding die. Case 1 takes second place. Cases 2 and 3 have relatively desirable stress distributions. As for Case 3, since the sliding insert is unfixed after the first stroke, the stress on Features A and B is released, so the stress on these features of the final part is very low.

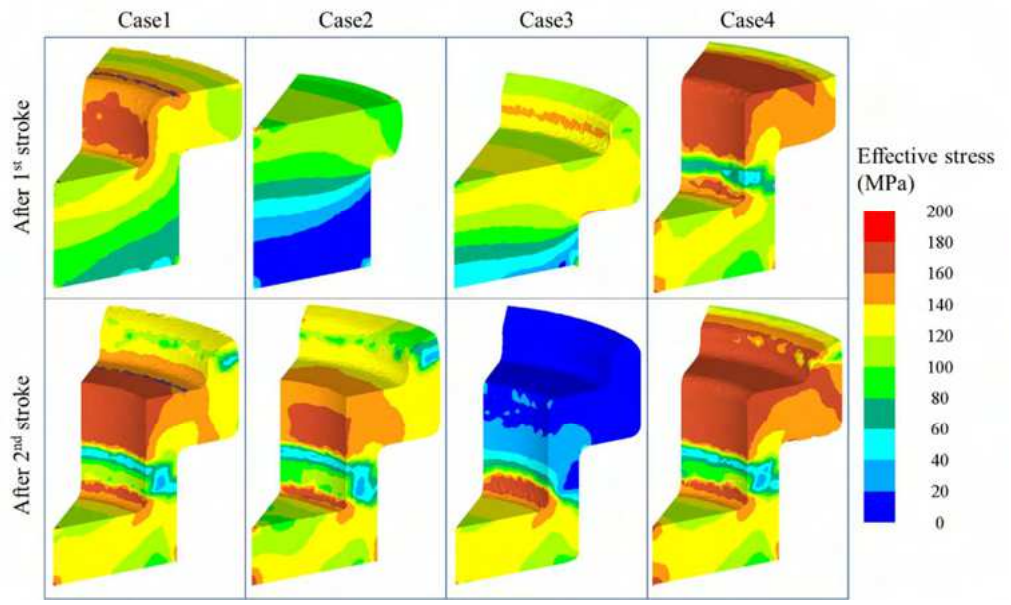

Fig. 20 Effective stress distribution after each stroke in Cases 1 to 4 revealed by simulation.

The top surface of Feature A is a freeform surface, that has no constraint from the punch or die. The shape of freeform surface is formed based on the interactive effect of internal deformation and friction, and it is required subsequent processes to obtain the desired geometry. The shapes and dimensions of Feature A are shown in **Fig. 21**, where H1 represents the height of Feature A, and H2 represents the height of the flat feature. As shown in **Fig. 21** (b), Case 3 has the highest H1 and H2, which represent the maximum allowance for subsequent processes. Since the material in Case 3 flows to form Feature A first, the material has less deformation accumulation so that it can flow upward more. Moreover, the other cases have the similar H2 values, and Case 4 has the lowest H1. Overall, Case 3 has the best performance in the freeform geometries.

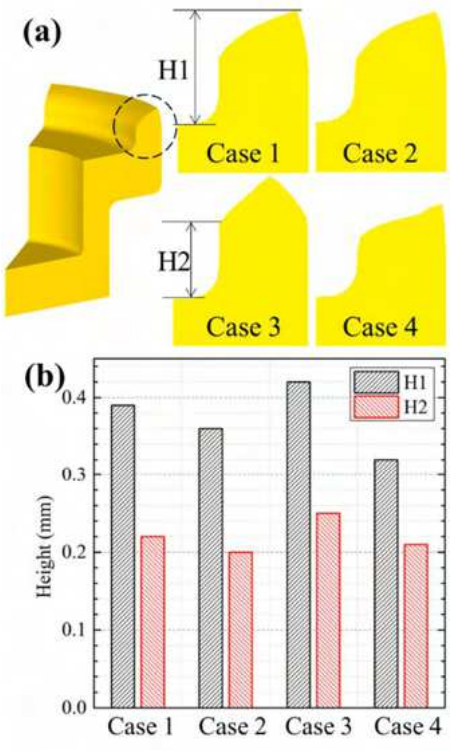

Fig. 21 (a) Geometries of Feature A of different cases. (b) Heights of Feature A.

Based on the simulation results, the advantages and disadvantages of the proposed design cases are summarized in **Table 3**. Case 1 has the limitation of head length for folding avoidance. Case 3 requires complicated forming fixations. Case 4 needs complicated die structures. Thus, the conventional one-stroke flange forming is changed to the upsetting-extrusion forming of Case 2 for experiments, which has moderate forming load and energy consumption.

Table 3 Advantages and disadvantages of different designs.

Improved designs	Advantages	Disadvantages
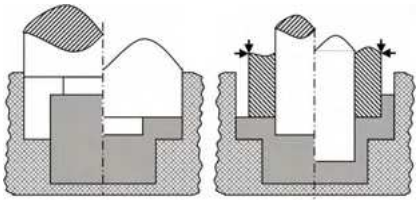 Case 1: Shortened-head design	• Simple punch and die; • Moderate forming load and energy	• Limit in folding avoidance; • Accurate volume-constant calculation; • Punch fixation

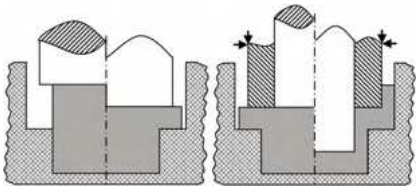 Case 2: Flat-punch design	• Simple punch and die; • Moderate forming load and energy	• Accurate volume-constant calculation; • Punch fixation
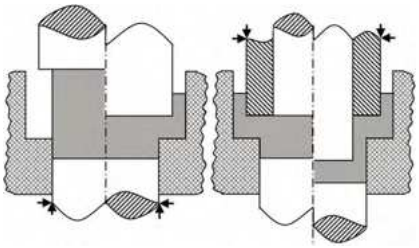 Case 3: Movable-die design	• Lower forming load; • Consume less energy; • Longer freeform	• Lower production efficiency; • Forming machine requirement; • Complicated forming fixation
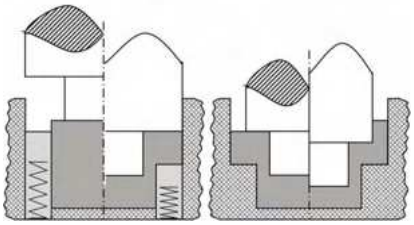 Case 4: Sliding-insert design	• Need not fix any die during forming	• Complicated die; • Higher forming load; • Consume more energy; • Shorter freeform

4.3 Morphologies of the experimental formed parts

The experimental tests of the conventional one-stroke forming and the improved forming of Case 2 were conducted to validate the reliability of the simulation results and feasibility of defect-free forming. The morphologies of the formed parts were observed by using a scanning electron microscope (SEM), a microscope, and a micro-lens camera, as shown in **Figs. 22–24**. These figures show that the design of Case 2 can feasibly avoid folding defects in all three size scales, which is consistent with the simulation results. Moreover, for the micro-and meso-scaled parts, the folding defects show irregularity around different locations, where some regions exhibit large defects, some exhibit small defects, and some show no defects. This phenomenon is caused by the increased inhomogeneous deformation of the material in the micro-/meso-scaled forming processes. Regarding the macro-scaled part in **Fig. 24**, the folding defect is much more severe compared with that in micro and meso scenarios and occurred regularly

around the cylindrical surface.

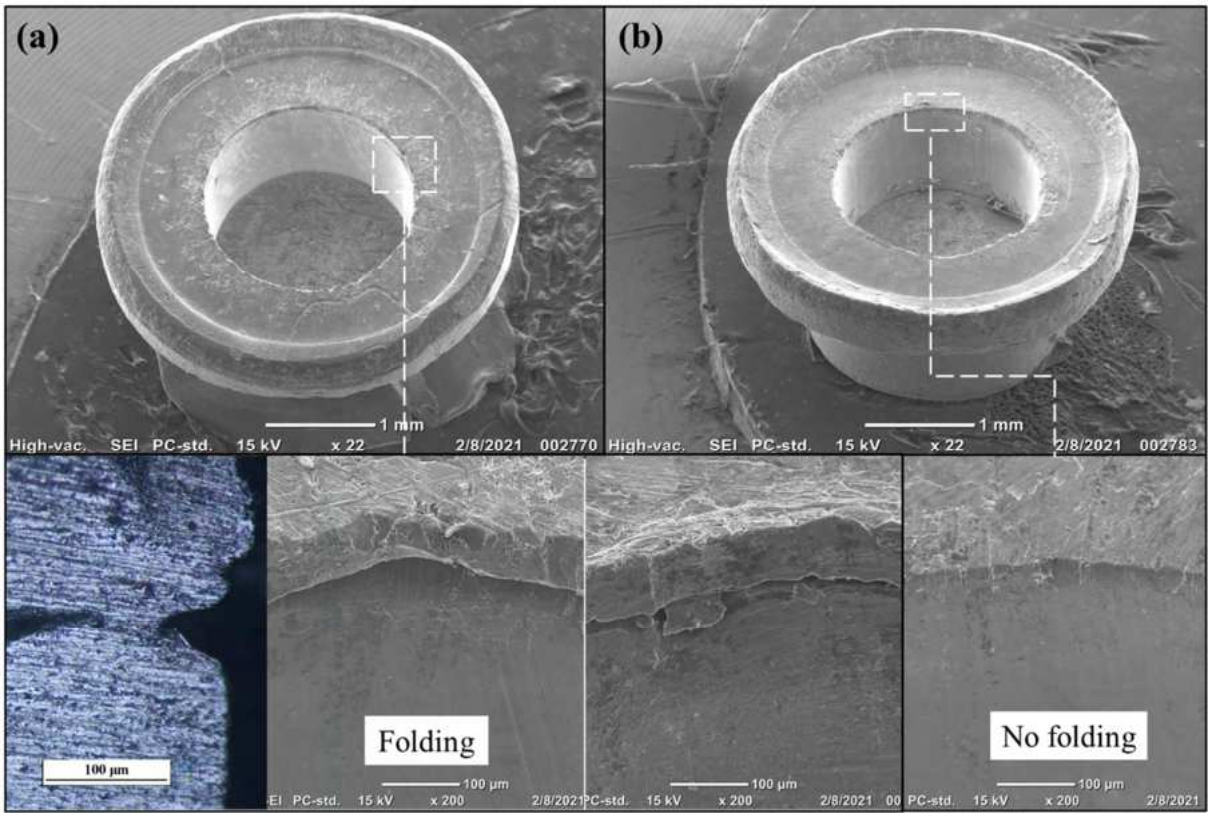

Fig. 22 The micro-scaled flanged parts formed by (a) one-stroke forming and (b) two-step forming in Case 2.

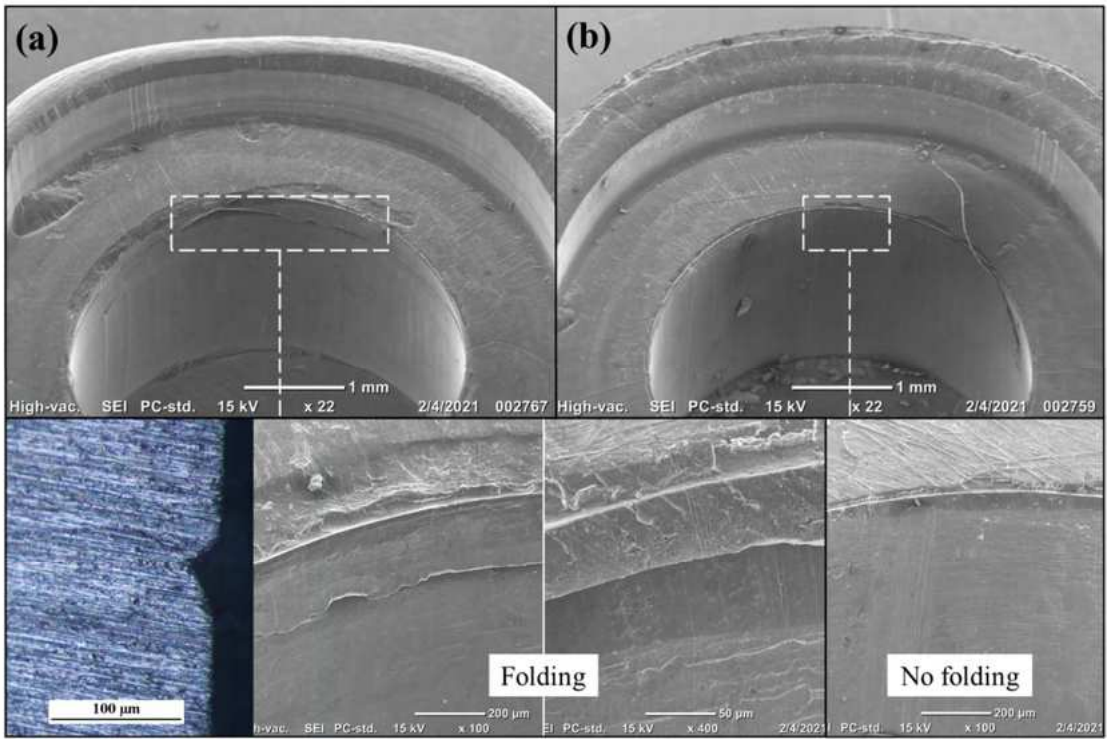

Fig. 23 The meso-scaled flanged parts formed by (a) one-stroke forming and (b) two-step forming in

Case 2.

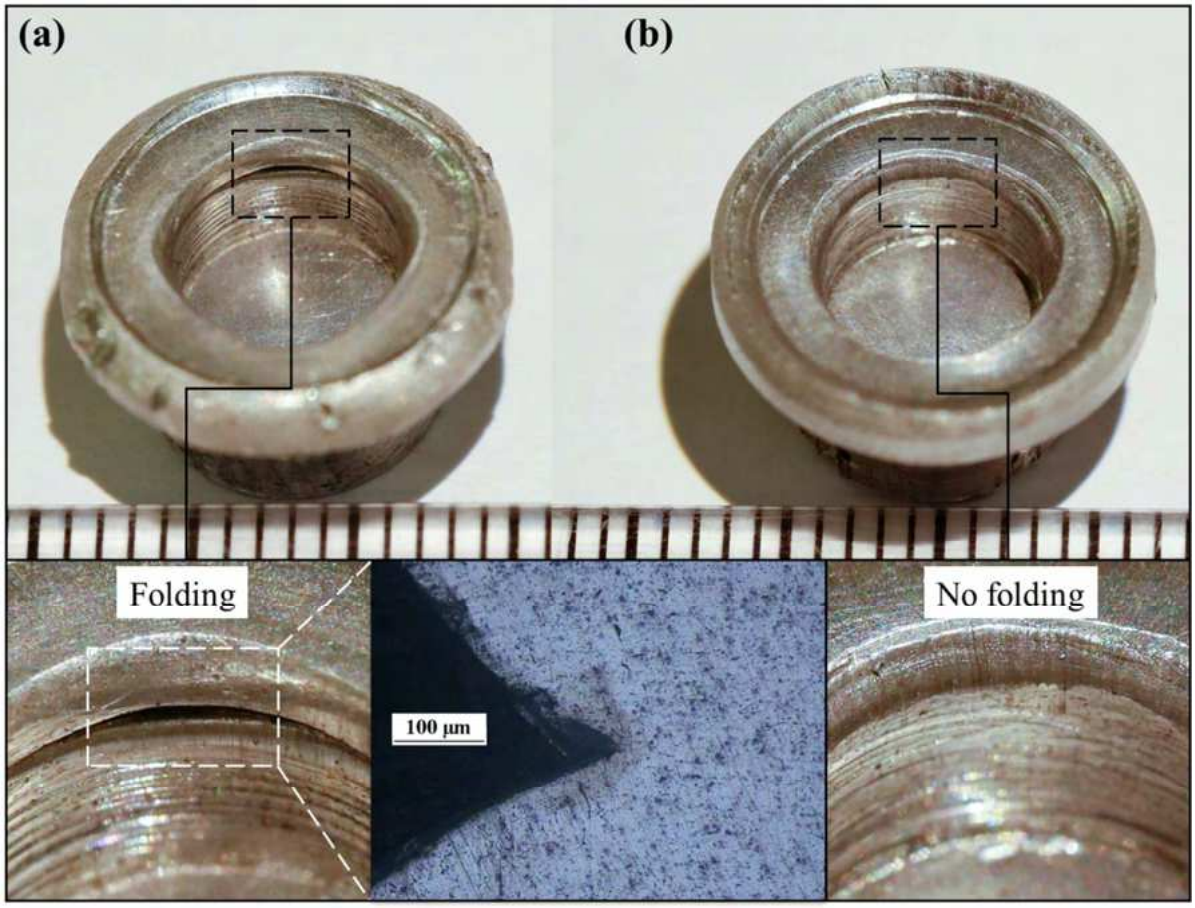

Fig. 24 The macro-scaled flanged parts formed by (a) one-stroke forming and (b) two-step forming of in Case 2.

5. Conclusions

Flow-induced folding is crucial in metal forming. Its formation mechanism and the relation with size effect were investigated in this research. A design-based approach for the analysis, prediction, and avoidance of folding defects was proposed, implemented, and validated. Based on the simulation and physical experiments of the proposed approach, the following concluding remarks are drawn:

1) Folding defects in axisymmetric bulk forming are flow-induced and structure-based as the result of material self-contact. The folding-free design of tooling and process to avoid material flow merging is an efficient way to avoid the initiation of folding defects.

2) In the axisymmetric multi-flanged part, folding is directly induced by the second contact of the punch shoulder during upsetting. Four improved design cases were established considering the forming sequence of three features of the part. The folding defect in Cases 2 to 4 can be avoided but Case 1 cannot. The infeasibility of Case 1 is related to the ratio of the shortened head length to its full length. When the shortened head is less than 55% of its full length, the folding defects can be avoided.
3) The movable-die design (Case 3) has the lowest forming load and consumed energy and the most desirable freeform geometries, but its stroke is larger and its total efficiency is lower. The flat-punch design (Case 2) has a good overall performance, given its resource consumption, forming efficiency, stress and strain distribution, and freeform geometries.
4) In the three-scaled forming experiments, meso-scaled forming produced the largest normalized forming load. The forming load of the simulation is similar to that found in the experimental results. The folding-free morphology is well formed in the deformed parts of Case 2, which is consistent with the simulation results. Furthermore, the folding defect at the macroscale is large and regular but this defect at the meso/microscale is irregular with different extents.

Acknowledgments

The authors would like to acknowledge the funding support to this research from the projects of ZE1W and BBAT from The Hong Kong Polytechnic University, the National Natural Science Foundation of China (NSFC) key project of No. 51835011, and the General Research Fund (GRF) project of 15223520.

Declarations

Funding

This research was supported by the projects of ZE1W and BBAT from The Hong Kong Polytechnic University, the National Natural Science Foundation of China (NSFC) key project of No. 51835011, and the General Research Fund (GRF) project of 15223520.

Conflicts of interest

The author declares no competing interests

Availability of data and material

All the data and material are available upon request to the corresponding author.

Code availability

Not applicable

Authors' contributions

Jun-Yuan Zheng: conceptualization, methodology, investigation, validation, visualization, writing — original draft, and writing — review and editing. **J.Y.C Fang:** conceptualization, methodology, and investigation. **M.W. Fu:** conceptualization, supervision, resources, and writing — review and editing.

Ethics approval

Not applicable

Consent to participate

Not applicable

Consent for publication

Not applicable

References

[1] Merklein M, Allwood JM, Behrens BA, Brosius A, Hagenah H, Kuzman K, Mori K, Tekkaya AE, Weckenmann A (2012) Bulk forming of sheet metal. CIRP Ann 61(2): 725-745. https://doi.org/10.1016/j.cirp.2012.05.007

[2] Cao J, Brinksmeier E, Fu M, Gao RX, Liang B, Merklein M, Schmidt M, Yanagimoto J (2019) Manufacturing of advanced smart tooling for metal forming. CIRP Ann 68(2): 605-628. https://doi.org/10.1016/j.cirp.2019.05.001

[3] Do V-C, Pham Q-T, Kim Y-S (2017) Identification of forming limit curve at fracture in incremental sheet forming. Int J Adv Manuf Tech 92(9): 4445-4455. 10.1007/s00170-017-0441-8

[4] Hussain G, Gao L, Hayat N (2011) Forming Parameters and Forming Defects in Incremental Forming of an Aluminum Sheet: Correlation, Empirical Modeling, and Optimization: Part A. Mater. Manuf. Processes 26(12): 1546-1553. 10.1080/10426914.2011.552017

[5] Silva MB, Isik K, Tekkaya AE, Martins PA (2015) Fracture loci in sheet metal forming: a review. Acta Metallurgica Sinica (English Letters) 28(12): 1415-1425.

[6] Tan CJ, Ibrahim MS, Muhamad MR (2019) Preventing delayed cracks in SUS304 deep drawn cups using extreme blank holding forces aided by nanolubrication. Int J Adv Manuf Tech 100(5): 1341-1354. 10.1007/s00170-018-2772-5

[7] Ortega S, Papula S, Saukkonen T, Talonen J, Hänninen H (2015) Characterization of delayed cracking in deep-drawn Swift cups of metastable austenitic stainless steels. Fatigue Fract Eng M 38(1): 29-39. https://doi.org/10.1111/ffe.12206

[8] Gong F, Yang Z, Chen Q, Xie Z, Shu D, Yang J (2015) Influences of lubrication conditions and blank holder force on micro deep drawing of C1100 micro conical–cylindrical cup. Precision Engineering 42: 224-230. https://doi.org/10.1016/j.precisioneng.2015.05.004

[9] Wang G, Li Y, Liu S, Yang J, Yang M (2018) Micro deep drawing of T2 copper foil using proportional decreased tools. Int J Adv Manuf Tech 95(1): 277-285. 10.1007/s00170-017-1111-6

[10] Chanhee W, Hyung-gyu K, Lee S, Kim D, Park S, Yoon J (2019) Wrinkling prediction for GPa-grade steels in sheet metal forming process. Int J Adv Manuf Tech 102(9-12): 3849-3863. http://dx.doi.org/10.1007/s00170-019-03518-3

[11] Arentoft M, Wanheim T (1997) The basis for a design support system to prevent defects in forging. J Mater Process Tech 69(1): 227-232. https://doi.org/10.1016/S0924-0136(97)00023-X

[12] Balendra R, Qin Y (2000) Identification and classification of flow-dependent defects in the injection forging of solid billets. J Mater Process Tech 106(1): 199-203. https://doi.org/10.1016/S0924-0136(00)00614-2

[13] Bao Y, Wierzbicki T (2004) A Comparative Study on Various Ductile Crack Formation Criteria. J. Eng. Mater. Technol. 126(3): 314-324. 10.1115/1.1755244

[14] Zhu S, Zhuang X, Xu D, Zhu Y, Zhao Z (2019) Flange forming at an arbitrary tube location through upsetting with a controllable deformation zone. J Mater Process Tech 273: 116230. https://doi.org/10.1016/j.jmatprotec.2019.05.011

[15] Wang JL, Fu MW, Ran JQ (2014) Analysis of size effect on flow-induced defect in micro-scaled forming process. Int J Adv Manuf Tech 73(9-12): 1475-1484. 10.1007/s00170-014-5947-8

[16] Sieczkarek P, Wernicke S, Gies S, Martins PAF, Tekkaya AE (2016) Incipient and repeatable plastic flow in incremental sheet-bulk forming of gears. Int J Adv Manuf Tech 86(9): 3091-3100. 10.1007/s00170-016-8442-6

[17] Abdullah AB, Sapuan SM, Samad Z, Khaleed HMT, Aziz NA (2013) Numerical investigation of geometrical defect in cold forging of an AUV blade pin head. J Manuf Process 15(1): 141-150. https://doi.org/10.1016/j.jmapro.2012.11.003

[18] Fu M, Shang B (1995) Stress analysis of the precision forging die for a bevel gear and its optimal design using the boundary-element method. J Mater Process Tech 53(3): 511-520. https://doi.org/10.1016/0924-0136(94)01754-O

[19] Fu MW, Yong MS, Tong KK, Muramatsu T (2006) A methodology for evaluation of metal forming system design and performance via CAE simulation. International Journal of Production Research 44(6): 1075-1092. 10.1080/00207540500337643

[20] Chan WL, Fu MW, Lu J (2010) FE Simulation-Based Folding Defect Prediction and Avoidance in Forging of Axially Symmetrical Flanged Components. Journal of Manufacturing Science and Engineering 132(5). 10.1115/1.4002188

[21] Chan WL, Fu MW, Lu J, Chan LC (2009) Simulation-enabled study of folding defect formation and avoidance in axisymmetrical flanged components. J Mater Process Tech 209(11): 5077-5086. https://doi.org/10.1016/j.jmatprotec.2009.02.005

[22] Sun Z, Cao J, Qiu H, Zhang C, Zhang H (2019) Determination of multi-direction loading

path based on analytical method in forming of multi-cavity parts by considering folding defect. Int J Adv Manuf Tech 100(1): 475-483. 10.1007/s00170-018-2751-x

[23] Gao PF, Yang H, Fan XG, Lei PH (2015) Quick prediction of the folding defect in transitional region during isothermal local loading forming of titanium alloy large-scale rib-web component based on folding index. J Mater Process Tech 219: 101-111. https://doi.org/10.1016/j.jmatprotec.2014.11.047

[24] Gao P, Yan X, Fei M, Zhan M, Li Y (2019) Formation mechanisms and rules of typical types of folding defects during die forging. Int J Adv Manuf Tech 104(1): 1603-1612. 10.1007/s00170-019-04145-8

[25] Gao PF, Fei MY, Yan XG, Wang SB, Li YK, Xing L, Wei K, Zhan M, Zhou ZT, Keyim Z (2019) Prediction of the folding defect in die forging: A versatile approach for three typical types of folding defects. J Manuf Process 39: 181-191. https://doi.org/10.1016/j.jmapro.2019.02.027

[26] Hsu C-C, Huang J-H, Chen W-C, Fuh Y-K (2017) Numerical analysis and experimental validation on multi-stage warm forging process of deep groove ball bearing—a modified punch geometry with microstructure and defect analysis. Int J Adv Manuf Tech 89(5): 2119-2128. 10.1007/s00170-016-9218-8

[27] Wang JL, Fu MW, Ran JQ (2013) Analysis and avoidance of flow-induced defects in meso-forming process: simulation and experiment. Int J Adv Manuf Tech 68(5): 1551-1564. 10.1007/s00170-013-4942-9

[28] Wang J, Fu M, Yu J, Wang X, Yang W (2016) Study of the flow behavior and defect formation in forming of axisymmetrically flanged and multi-scaled parts. Int J Precis Eng Man 17(10): 1341-1349. 10.1007/s12541-016-0159-9

[29] Wang JL, Fu MW, Ran JQ (2014) Analysis of size effect on flow-induced defect in micro-scaled forming process. Int J Adv Manuf Tech 73(9): 1475-1484. 10.1007/s00170-014-5947-8

[30] Liu Y, Wu Y, Wang J, Liu S (2018) Defect analysis and design optimization on the hot forging of automotive balance shaft based on 3D and 2D simulations. Int J Adv Manuf Tech 94(5): 2739-2749. 10.1007/s00170-017-1080-9

[31] Zhu S, Zhuang X, Zhu Y, Zhao Z (2018) Thickening of cup sidewall through sheet-bulk forming with controllable deformation zone. J Mater Process Tech 262: 597-604. https://doi.org/10.1016/j.jmatprotec.2018.07.036

[32] Swift HW (1952) Plastic instability under plane stress. J Mech Phys Solids 1(1): 1-18. https://doi.org/10.1016/0022-5096(52)90002-1

[33] Lai X, Peng L, Hu P, Lan S, Ni J (2008) Material behavior modelling in micro/meso-scale forming process with considering size/scale effects. Comput Mater Sci 43(4): 1003-1009. https://doi.org/10.1016/j.commatsci.2008.02.017

[34] Pradeep Raja C, Ramesh T (2021) Influence of size effects and its key issues during microforming and its associated processes – A review. Eng Sci Technol an Int J 24(2): 556-570. https://doi.org/10.1016/j.jestch.2020.08.007